Contrib Mineral Petrol (2005) 149: 338–349
DOI 10.1007/s00410-005-0653-z

ORIGINAL PAPER

O. Bachmann · M. A. Dungan · F. Bussy

# Insights into shallow magmatic processes in large silicic magma bodies: the trace element record in the Fish Canyon magma body, Colorado

Received: 19 August 2004 / Accepted: 31 January 2005 / Published online: 9 March 2005


**Abstract** Highly evolved rhyolite glass plus near-solidus mineral assemblages in voluminous, dacitic, crystal-rich ignimbrites provide an opportunity to evaluate the late magmatic evolution of granodiorite batholiths. This study reports laser-ablation ICP-MS analyses of trace element concentrations in feldspars, hornblende, biotite, titanite, zircon, magnetite, and interstitial glass of the crystal-rich Fish Canyon Tuff. The high-silica rhyolite glass is characterized by relatively high concentrations of feldspar-compatible elements (e.g., 100 ppm Sr and 500 ppm Ba) and low concentrations of Y (< 7 ppm) and HREE (~1 ppm Yb), hence high LREE/HREE (Ce/Yb > 40) compared to many well-studied high-silica rhyolite glasses and whole-rock compositions. Most minerals record some trace element heterogeneities, with, in particular, one large hornblende phenocryst showing four- to six-fold core-to-rim increases in Sr and Ba coupled with a decrease in Sc. The depletions of Y and HREE in the Fish Canyon glass relative to the whole-rock composition (concentrations in glass ~30% of those in whole rocks) reflect late crystallization of phases wherein these elements were compatible. As garnet is not stable at the low-P conditions at which the Fish Canyon magma crystallized, we show that a combination of modally abundant hornblende (~4%) + titanite (~0.5–1%) and the highly polymerized nature of the rhyolitic liquid led to Y and HREE depletions in melt. Relatively high Sr and Ba contents in glass and rimward Sr and Ba increases in euhedral, concentrically zoned hornblende suggest partial feldspar dissolution and a late release of these elements to the melt as hornblende was crystallizing, in agreement with textural evidence for feldspar (and quartz) resorption. Both observations are consistent with thermal rejuvenation of the magma body prior to eruption, during which the proportion of melt increased via feldspar and quartz dissolution, even as hydrous and accessory phases were crystallizing. Sr/Y in Fish Canyon glass (13–18) is lower than the typical "adakitic" value (> 40), confirming that high Sr/Y is a reliable indicator of high-pressure magma generation and/or differentiation wherein garnet is implicated.

Editorial Responsibility: T.L. Grove

O. Bachmann (✉) · M. A. Dungan
Section des Sciences de la Terre,
Université de Genève, 13, rue des maraîchers,
1211 Genève 4, Switzerland
E-mail: olivier.bachmann@terre.unige.ch
Tel.: +4122-3796893
Fax: +4122-3793210
E-mail: michael.dungan@terre.unige.ch

F. Bussy
Faculté des géosciences et de l'environnement,
Université de Lausanne, Switzerland
E-mail: Francois.Bussy@unil.ch

## Introduction

Voluminous, homogeneous, crystal-rich, dacitic ignimbrites (monotonous intermediates of Hildreth 1981) are important for the understanding of magmatic processes involved in the formation and evolution of the upper crust because they provide a unique window into the evolution of large granodioritic magma bodies. They represent batholiths erupted in a state near "viscous death" (near the rheological transition from liquid to solid), thereby avoiding the blurring effects of the time-integrated histories recorded in plutons (e.g., multiple intrusive events, post-intrusion deformation, subsolidus overprints). The preservation of interstitial melt compositions in such volcanic rocks, as glass, provides insights into near-solidus magmatic processes in large silicic magma bodies.

In previous studies of the archetypal monotonous intermediate, the ~5,000 $km^3$ Fish Canyon Tuff, San Juan volcanic field, Colorado (Lipman et al. 1997; Bachmann et al. 2002), we noted that the concentrations of feldspar-compatible elements such as Eu, Sr, and Ba are higher in the interstitial glass than would be

predicted if feldspars had been crystallizing immediately prior to eruption at these near-solidus conditions, whereas Y and HREE are lower in the glass than in the whole-rock composition. As the Fish Canyon magma evolved in a shallow crustal reservoir (2.2–2.5 kbar) at near-solidus temperatures (700–760°C; Johnson and Rutherford 1991; Bachmann and Dungan 2002) and it records the coexistence of 11 mineral phases (Pl + Kfs + Qtz + Hbl + Bt + Ttn + Mag + Ilm + Ap + Zrn + Po) with high-$SiO_2$ rhyolite melt (76 wt% $SiO_2$), observed depletions of Y and HREE in glass cannot be the consequence of garnet crystallization in the Fish Canyon magma chamber. Consequently, we have documented the trace element budget of the Fish Canyon magma through laser-ablation ICP-MS analyses of glass and mineral phases, including trace element zoning in hornblende, in order to further elucidate the immediately pre-eruptive evolution of this upper-crustal, batholithic-scale, granodioritic magma body.

## Fish Canyon magma

The Fish Canyon magma body was tapped by three closely related eruptions at ~28 Ma (Lipman et al. 1997; Bachmann et al. 2000; Lipman 2000). From oldest to youngest, these volcanic units are: (1) the ~200 $km^3$ Pagosa Peak Dacite, a fountain-fed, poorly fragmented, pyroclastic unit, (2) the climactic, ~5,000 $km^3$ Fish Canyon Tuff, and (3) the < 1 $km^3$ Nutras Creek Dacite, a lava flow marking the end of the Fish Canyon magmatic cycle. These three units are strikingly homogeneous in whole-rock chemistry (~68 ± 0.5 wt% $SiO_2$) and mineralogy. Crystallinity is high (~45 vol% crystals), and the 11-phase mineral assemblage is typical of granodiorite plutons (in particular, the presence of amphibole + titanite is uncommon in erupted arc magmas; Nakada 1991; Deer et al. 1992). The matrix of this near-solidus assemblage is commonly devitrified, although glassy basal vitrophyres are present in both the Fish Canyon Tuff and in the Pagosa Peak Dacite. Quartz, sanidine, and some plagioclase crystals are deeply corroded, whereas the other phases are euhedral. This observation, along with other textural and geochemical evidence (see Bachmann and Dungan 2002; Bachmann et al. 2002), suggest simultaneous dissolution of feldspars + quartz and crystallization of hydrous phases (hornblende, biotite, titanite) during gradual near-isobaric reheating (from ~710 to 760°C) of the magma body. We have postulated that thermal rejuvenation was engendered by the intrusion of hot, volatile-rich mafic magma at the base a crystalline mush (Bachmann et al. 2002). Similar interpretations have been proposed for magmatic systems, such as the ongoing eruption at Soufrière Hills volcano, Montserrat, W.I. (Murphy et al. 2000; Devine et al. 2003; Rutherford and Devine 2003) and the 1980–1986 eruption of Mount St. Helens, USA (Rutherford 2002), suggesting that thermal rejuvenation and remobilization of near-solidus mushes may be common over a wide range of magma volumes.

In order to account for reheating of volumes of magma as large as the Fish Canyon body on reasonable time scales (~$10^5$ years) and to keep hydrous phases stable during reheating, Bachmann and Bergantz (2003) suggested that efficient heat transfer from the mafic to the silicic magma may have been abetted by upward percolation through the crystal mush of a solute-rich hydrous fluid exsolved from the underplated mafic intrusion. Such an ascending fluid almost certainly would have entrained some relatively mafic melt upon escape from the underlying magma, thereby leading to modest replenishments of Fe, Ti, Mg, and Ca. The transfer of this melt, along with heat and volatiles, was essential to the growth of such phases as biotite, titanite, and hornblende at the same time that alkali feldspar and quartz were dissolving. Previously documented rimward increases in fluorine contents of biotite phenocrysts are in accord with this process (Bachmann et al. 2002). Entrainment of small quantities of mafic melt by the percolating fluid phase, rather than more thorough mingling (as suggested by the scarcity of andesitic enclaves in the Fish Canyon system; Bachmann et al. 2002) would facilitate blending, leading to reprecipitation of the mafic components on pre-existing minerals. In addition to the euhedral hornblende phenocrysts that record reverse thermal zoning in the form of increasing edenite component toward their rims (Bachmann and Dungan 2002), many plagioclase crystals in Fish Canyon eruptive products display euhedral, oscillatory-zoned overgrowths that are characterized by narrow calcic "spikes" and overall reverse zoning profiles ($An_{27-28}$ to $An_{32-34}$) indicative of up-temperature, open-system crystallization (Bachmann et al. 2002). The present study was in large part undertaken to further test the hypothesis of volatile-driven thermal rejuvenation of the Fish Canyon magma body.

## Sample preparation and analysis

Laser-ablation ICP-MS analyses (with pit site diameters of 30–60 μm) were performed on plagioclase, sanidine, hornblende, biotite, magnetite, zircon, titanite, and glass from three vitrophyric samples, corresponding to different stratigraphic levels in the Fish Canyon magmatic system. These are: (1) the early erupted Pagosa Peak Dacite (Bfc 83), (2) the outflow Fish Canyon Tuff (Bfc 113), and the late-erupted intracaldera Fish Canyon Tuff (Bfc 191). These analyses were done on 90-μm thick sections for all phases but zircon and titanite, for which we used separated polished crystals from one sample of the Pagosa Peak Dacite (Bfc 15) that we mounted in epoxy and ablated with the laser. We also analyzed zircon and titanite in cognate xenoliths collected from the intracaldera Fish Canyon Tuff (the granodioritic Mlx12 for titanite, and the granitic GrnX for zircons,

both having the same U–Pb ages as the Fish Canyon magma; Bachmann et al. submitted). Although apatite is present and may contain significant amounts of Y, REE, and Sr, its low modal abundance and occurrence mainly as tiny acicular inclusions in hornblende and biotite rendered analyses impossible with a laser ablation pit $>10$ μm.

The measurements were acquired with a 193 nm Lambda Physics Excimer laser (Geolas 200 M system) coupled to a Perkin-Elmer 6100 DRC ICP-MS. Laser settings were 27 kV and 10 Hz repetition rate, yielding a fluence of about 12 J/cm$^2$ on the ablation site. Helium was used as carrier gas (1.1 l/min). We chose NIST610 and 612 glasses as external standards, and Ca and Si as internal standards (on the basis of electron microprobe measurements on the ablation pit site). BCR2 basaltic glass was regularly used as a monitor to check for reproducibility and accuracy of the system. Results were always within $\pm 10\%$ of the values reported by Witt-Eickschen et al. (2003); Rb, Cs, Y, and Cr were sometimes out of the $\pm 10\%$ range of the USGS recommended values for BCR2g. Wherever possible, several spots were analyzed for each phase to document the trace element variability within individual crystals and between crystals of the same thin section. Data reduction was done using standard Perkin Elmer software, or LAMTRACE, a spreadsheet developed by S.E. Jackson (Macquarie University, Sydney).

## Results

### Trace element contents of Fish Canyon minerals and glass

For most elements (in particular, those with concentrations $>5$ ppm), the glass analyses from all three samples yield similar concentrations and low variability. Fe, Mg, Li, and S are the only elements to display larger relative standard deviations (Table 1). Variations in Fe and Mg concentrations are probably related to incipient glass devitrification, which occurs in the form of minute oxide filaments (Bachmann et al. 2002), and produces local heterogeneities in these elements. Variability in the volatile elements Li and S (see also Cl variations in whole-rock composition; Bachmann et al. 2002) is also expected in this 28 Ma old glass, as some post-emplacement hydration (or volatile exchange) must have occurred. We note that trace element concentrations determined by ion microprobe on a glassy sample of Pagosa Peak Dacite compare well with the ICP-MS data (see Table 8 of Bachmann et al. 2002).

The concentrations of most trace elements in all analyzed mineral phases show significant variations, in most cases larger than measured values of the same element in the glass. Although this could be partly due to the smaller number of analyses in each crystalline

**Table 1** Trace element concentrations (ppm) in glasses from the Fish Canyon magmatic system

| | Bfc 83 (PPD) | | | Bfc 113 (FCT-O) | | | Bfc 191 (FCT-I) | | |
|---|---|---|---|---|---|---|---|---|---|
| | Average, $N=16$ | SD | Rel. SD (%) | Average, $N=16$ | SD | Rel. SD (%) | Average, $N=12$ | SD | Rel. SD (%) |
| Li | 30 | 8 | 25 | 35 | 8 | 22 | 35 | 16 | 44 |
| Mg | 425 | 35 | 8 | 557 | 216 | 39 | 528 | 249 | 47 |
| P | 21 | 7 | 32 | 15 | 5 | 33 | 26 | 11 | 42 |
| S | 11 | 36 | 316 | 11 | 6 | 57 | n.m. | n.m. | n.m. |
| Sc | 2.8 | 0.5 | 17 | 3.0 | 0.4 | 12 | 3.1 | 0.2 | 6 |
| Cr | $<0.01$ | – | – | 0.2 | 2.1 | 1,050 | 0.5 | 0.4 | 80 |
| Fe | 4,275 | 4,709 | 110 | 5,148 | 1,249 | 24 | 4,537 | 429 | 9 |
| Ni | 0.1 | 0.4 | 323 | 0.4 | 0.3 | 76 | 0.3 | 0.2 | 55 |
| Rb | 182 | 4 | 2 | 209 | 5 | 2 | 187 | 1 | 1 |
| Sr | 93 | 2 | 2 | 115 | 16 | 13 | 77 | 2 | 3 |
| Y | 6.9 | 0.3 | 4 | 7.1 | 1.4 | 19 | 5.8 | 0.2 | 4 |
| Zr | 83 | 2 | 2 | 86 | 14 | 16 | 70 | 2 | 3 |
| Nb | 14.4 | 0.5 | 3 | 16.4 | 0.3 | 2 | 13.6 | 0.3 | 2 |
| Cs | 5.2 | 0.1 | 2 | 5.9 | 0.2 | 3 | 4.7 | 0.1 | 2 |
| Ba | 336 | 4 | 1 | 589 | 63 | 11 | 414 | 9 | 2 |
| La | 36.2 | 0.7 | 2 | 37.3 | 5.5 | 15 | 29.8 | 0.9 | 3 |
| Ce | 46.1 | 0.6 | 1 | 52.3 | 2.6 | 5 | 40.8 | 1.1 | 3 |
| Nd | 10.5 | 0.6 | 6 | 10.9 | 1.5 | 14 | 8.6 | 0.4 | 5 |
| Sm | 1.39 | 0.21 | 15 | 1.47 | 0.36 | 24 | 1.14 | 0.14 | 12 |
| Eu | 0.29 | 0.05 | 17 | 0.34 | 0.05 | 15 | 0.28 | 0.03 | 11 |
| Gd | 1.11 | 0.2 | 18 | 1.22 | 0.26 | 21 | 1.07 | 0.1 | 9 |
| Dy | 0.91 | 0.11 | 12 | 1.01 | 0.23 | 23 | 0.76 | 0.06 | 8 |
| Er | 0.7 | 0.08 | 11 | 0.76 | 0.17 | 22 | 0.59 | 0.06 | 10 |
| Yb | 1.1 | 0.15 | 14 | 1.07 | 0.32 | 30 | 0.94 | 0.07 | 7 |
| Hf | 2.97 | 0.31 | 10 | 3 | 0.56 | 19 | 2.39 | 0.19 | 8 |
| Ta | 1.05 | 0.06 | 6 | 1.17 | 0.1 | 9 | 0.98 | 0.04 | 4 |
| Pb | 20.9 | 0.6 | 3 | 24.2 | 0.7 | 3 | 21.7 | 0.9 | 4 |
| Th | 22.9 | 0.4 | 2 | 22.6 | 3.4 | 15 | 18.6 | 0.6 | 3 |
| U | 8.46 | 0.19 | 2 | 9.65 | 0.23 | 2 | 7.38 | 0.12 | 2 |

For all tables, the average and standard deviation (SD, 1$\sigma$ per sample) was calculated using the total number of points ($N$) made in this particular sample. The reported SD is much larger than the analytical SD (typically, 1–5% of the measurement) and provides information on the chemical variability in the sample (within a crystal and between different crystals; Rel. SD is the relative SD). *n.m.* not measured, *PPD* Pagosa Peak Dacite, *FCT-O* Outflow Fish Canyon Tuff, *FCT-I* Intracaldera Fish Canyon Tuff.

phase, and lower yields for feldspars compared to glass and ferromagnesian minerals, it implies the existence of heterogeneities or zoning, at least for elements in relatively high concentrations (i.e., Sr and Ba in most phases, Sc and Ce in hornblende). We note that each sample (wherein multiple spots in several crystals were analyzed) shows similar average concentrations for most trace elements (Tables 2, 3, 4, 5, 6, 7, and 8). For example, Sr and Ba display relative standard deviations >10% but similar average concentrations for various mineral phases in all three samples. This observation is consistent with textural complexities and major element zoning in Fish Canyon minerals (Bachmann et al. 2002; see also cathodoluminescence images of zircons and titanite of Schmitz and Bowring 2001). As chemical variations generally occur on a finer scale than the spot size of the laser, most analyses are mixtures of multiple zones. Therefore, apart from the exception of one large hornblende grain (see below), these analyses cannot be used to resolve mineral zoning.

Determinations of average trace element concentrations in minerals and glass permit an assessment of first-order partitioning behavior between crystals and melt (Fig. 1 and Table 9). However, due to the multiple limitations of the phenocryst-matrix technique for determining accurate partition coefficients (e.g., Irving and Frey 1978; Irving and Frey 1984), which would be particularly severe for the Fish Canyon magma due to significant intra-grain zonations and inter-grain differences, the analytical results that we report for minerals cannot be converted to true partition coefficients. We use the notation $\check{C}_{\text{i-min.}}$ (average concentration of $i$ from multiple analyses of multiple grains in a sample) to specify the average concentration of an element ($i$) in a particular mineral phase, and the formulation $\check{C}_{\text{i-min}}/\check{C}_{\text{i-melt}}$ as an index of partitioning behavior that is analogous to, but far less precise than experimentally determined partition coefficients.

These indices of partitioning behavior ($\check{C}_{\text{i-min}}/\check{C}_{\text{i-melt}}$; Table 9) have been used to draw conclusions about the trace element budget of the Fish Canyon magma. Using the whole-rock concentrations of an element and its average concentration ($\check{C}_{\text{i}}$) in each phase (minerals and glass), one can verify the analytically determined (by ICP-MS) trace element budget by comparison to petrographically measured modal abundances. Knowing the concentration of an element in the whole rock and its average concentration in each phase, the proportions of the different minerals can be estimated by least-squares fitting. These calculated modes, which are similar to the petrographic modes (thin section point counting; Table 10), confirm that the trace element budget is approximately balanced using the reported modal abundances and measured concentrations, even without taking into account apatite.

Values of $\check{C}_{\text{i-min}}/\check{C}_{\text{i-melt}}$ (Table 9 and Fig. 2) are generally high to very high in the Fish Canyon magma compared to published values of equilibrium partition

**Table 2** Trace element concentrations (ppm) in sanidines from the Fish Canyon magmatic system

| | Bfc 83 (PPD) | | | Bfc 113 (FCT-O) | | | Bfc 191 (FCT-I) | | |
|---|---|---|---|---|---|---|---|---|---|
| | Average, $N=9$ | SD | Rel. SD (%) | Average, $N=5$ | SD | Rel. SD (%) | Average, $N=6$ | SD | Rel. SD (%) |
| Li | n.m. | n.m. | n.m. | 0.52 | 0.27 | 51 | 0.57 | 0.26 | 45 |
| Mg | 7 | 3 | 37 | 7 | 2 | 25 | 7 | 1 | 15 |
| S | n.m. | n.m. | n.m. | 5.8 | 2.41 | 42 | n.m. | n.m. | n.m. |
| Sc | 1.0 | 0.2 | 22 | 1.5 | 0.3 | 21 | 1.6 | 0.2 | 10 |
| Cr | 0.5 | 2.4 | 449 | <0.01 | – | – | 1.3 | 0.6 | 45 |
| Fe | 833 | 33 | 4 | 780 | 33 | 4 | 836 | 56 | 7 |
| Ni | n.m. | n.m. | n.m. | 0.1 | 0.1 | 100 | 0.1 | 0.2 | 169 |
| Rb | 147 | 10 | 7 | 135 | 6 | 4 | 130 | 5 | 4 |
| Sr | 686 | 156 | 23 | 685 | 85 | 12 | 731 | 134 | 18 |
| Y | 0.4 | 0.1 | 24 | 0.2 | 0.1 | 50 | 0.3 | 0.2 | 46 |
| Zr | <0.01 | – | – | 0.03 | 0.04 | 145 | 0.01 | 0.01 | 92 |
| Nb | <0.01 | – | – | <0.02 | – | – | <0.01 | – | – |
| Cs | n.m. | n.m. | n.m. | 0.15 | 0.02 | 16 | 0.17 | 0.02 | 10 |
| Ba | 7,861 | 1,537 | 20 | 7,553 | 1,503 | 20 | 7,540 | 3,043 | 40 |
| La | 2.24 | 0.45 | 20 | 2.07 | 0.4 | 19 | 2.22 | 0.45 | 20 |
| Ce | 1.0 | 0.2 | 23 | 1.1 | 0.4 | 38 | 1.0 | 0.2 | 22 |
| Nd | 0.12 | 0.06 | 49 | 0.09 | 0.05 | 61 | 0.07 | 0.05 | 71 |
| Sm | <0.01 | – | – | <0.01 | – | – | <0.01 | – | – |
| Eu | 0.9 | 0.18 | 20 | 0.84 | 0.04 | 4 | 0.92 | 0.13 | 14 |
| Gd | 0.09 | 0.07 | 80 | 0.09 | 0.05 | 55 | 0.27 | 0.11 | 41 |
| Dy | 0.03 | 0.09 | 307 | <0.01 | – | – | <0.01 | – | – |
| Er | <0.02 | – | – | <0.02 | – | – | <0.02 | – | – |
| Yb | 0.08 | 0.09 | 119 | 0.02 | 0.01 | 71 | 0.01 | 0.01 | 108 |
| Hf | 0.3 | 0.19 | 63 | 0.27 | 0.09 | 34 | 0.31 | 0.14 | 47 |
| Ta | 0.32 | 0.08 | 27 | 0.43 | 0.1 | 24 | 0.33 | 0.1 | 29 |
| Pb | 25.3 | 5.4 | 21 | 23.8 | 1.6 | 7 | 22.2 | 2.1 | 9 |
| Th | <0.01 | – | – | <0.01 | – | – | <0.01 | – | – |
| U | <0.01 | – | – | <0.01 | – | – | <0.01 | – | – |

**Table 3** Trace element concentrations (ppm) in plagioclases from the Fish Canyon magmatic system

| | Bfc 83 (PPD; core) | | | Bfc 83 (PPD; rim) | | | Bfc 113 (FCT-O) | | | Bfc 191 (FCT-I) | | |
|---|---|---|---|---|---|---|---|---|---|---|---|---|
| | Average, $N=3$ | SD | Rel. SD (%) | Average, $N=5$ | SD | Rel. SD (%) | Average, $N=8$ | SD | Rel. SD (%) | Average, $N=6$ | SD | Rel. SD (%) |
| Li | 7.3 | 2.4 | 33 | 3.4 | 0.2 | 6 | 5.3 | 0.5 | 10 | 5.0 | 1.4 | 28 |
| Mg | 214 | 78 | 37 | 143 | 1 | 1 | 115 | 78 | 68 | 77 | 39 | 51 |
| P | 6.2 | 8.6 | 139 | 40.9 | 8.7 | 21 | 14.6 | 11.0 | 75 | 21.6 | 16.0 | 74 |
| S | 14.2 | 4.0 | 28 | 7.4 | 1.9 | 25 | 7.3 | 3.9 | 54 | n.m. | n.m. | n.m. |
| Sc | 3.5 | 1.2 | 34 | 0.2 | 0.2 | 111 | 0.3 | 1.0 | 317 | 1.5 | 0.3 | 23 |
| Cr | < 0.01 | – | – | 1 | 3 | 231 | 3 | 3 | 100 | < 0.01 | – | – |
| Fe | 2,026 | 125 | 6 | 2,187 | 570 | 26 | 2,655 | 913 | 34 | 1,609 | 188 | 12 |
| Ni | < 0.01 | – | – | < 0.01 | – | – | 3.1 | 6.8 | 223 | 0.1 | 0.1 | 89 |
| Rb | 2.3 | 0.6 | 26 | 0.7 | 0.0 | 3 | 1.9 | 0.4 | 20 | 1.1 | 0.6 | 50 |
| Sr | 1,243 | 32 | 3 | 1,205 | 83 | 7 | 1,144 | 60 | 5 | 1,165 | 206 | 18 |
| Y | 0.09 | 0.05 | 56 | 0.14 | 0.01 | 9 | 0.06 | 0.05 | 89 | 0.13 | 0.07 | 49 |
| Zr | 0.12 | 0.21 | 168 | 0.24 | 0.2 | 80 | 0.16 | 0.22 | 139 | 0.17 | 0.15 | 84 |
| Nb | 0.08 | 0.04 | 56 | 0.09 | 0.06 | 59 | 0.07 | 0.08 | 107 | 0.03 | 0.02 | 80 |
| Cs | < 0.01 | – | – | < 0.01 | – | – | < 0.01 | – | – | < 0.01 | – | – |
| Ba | 379 | 43 | 11 | 151 | 20 | 13 | 278 | 23 | 8 | 276 | 36 | 13 |
| La | 16.7 | 1.2 | 7 | 8.3 | 0.2 | 3 | 14.3 | 1 | 7 | 14.4 | 2.4 | 17 |
| Ce | 13.7 | 0.9 | 7 | 10.9 | 0.4 | 4 | 11.9 | 1.5 | 12 | 13.2 | 2.3 | 18 |
| Nd | 1.66 | 0.38 | 23 | 2.57 | 0.37 | 14 | 1.4 | 0.41 | 30 | 2.65 | 1.14 | 43 |
| Sm | 0.13 | 0.08 | 64 | 0.32 | 0.11 | 36 | 0.1 | 0.07 | 68 | 0.17 | 0.11 | 67 |
| Eu | 1.17 | 0.07 | 6 | 0.61 | 0.08 | 13 | 0.95 | 0.12 | 13 | 1.1 | 0.17 | 16 |
| Gd | 0.11 | 0.07 | 61 | 0.11 | 0.04 | 32 | 0 | 0.06 | 1,912 | 0.14 | 0.07 | 45 |
| Dy | < 0.01 | – | – | 0.02 | 0.02 | 103 | 0.04 | 0.02 | 63 | 0.03 | 0.02 | 72 |
| Er | < 0.02 | – | – | < 0.01 | – | – | < 0.01 | – | – | < 0.01 | – | – |
| Yb | < 0.02 | – | – | < 0.02 | – | – | < 0.02 | – | – | < 0.02 | – | – |
| Hf | < 0.02 | – | – | < 0.02 | – | – | < 0.02 | – | – | < 0.02 | – | – |
| Ta | < 0.01 | – | – | < 0.01 | – | – | < 0.01 | – | – | < 0.01 | – | – |
| Pb | 13.3 | 1.2 | 9 | 7.7 | 0.5 | 6 | 13.9 | 0.9 | 6 | 9.9 | 1.6 | 16 |
| Th | < 0.01 | – | – | < 0.01 | – | – | < 0.02 | – | – | < 0.02 | – | – |
| U | < 0.01 | – | – | 0.19 | 0.32 | 167 | 0.45 | 0.61 | 136 | < 0.01 | – | – |

**Table 4** Trace element concentrations (ppm) in hornblendes from the Fish Canyon magmatic system

| | Bfc 83 (PPD) | | | Bfc 113 (FCT-O) | | | Bfc 191 (FCT-I) | | |
|---|---|---|---|---|---|---|---|---|---|
| | Average, $N=7$ | SD | Rel. SD (%) | Average, $N=6$ | SD | Rel. SD (%) | Average, $N=3$ | SD | Rel. SD (%) |
| Li | 9.4 | 3.3 | 36 | 10.2 | 1.4 | 14 | 12.1 | 1.0 | 9 |
| P | 9 | 9 | 10 | 84 | 51 | 61 | 381 | 53 | 14 |
| S | 8 | 9 | 107 | 17 | 3 | 18 | n.m. | n.m. | n.m. |
| Sc | 181 | 13 | 7 | 107 | 12 | 11 | 111 | 5 | 5 |
| Cr | 1.9 | 2.9 | 155 | 6.9 | 2.6 | 38 | 2.6 | 1.0 | 40 |
| Ni | 11.4 | 2.2 | 19 | 12.2 | 0.8 | 7 | 13.6 | 2.8 | 21 |
| Rb | 2.7 | 1.4 | 52 | 3.5 | 2.3 | 65 | 2.3 | 0.1 | 2 |
| Sr | 19 | 4 | 23 | 56 | 20 | 35 | 44 | 11 | 26 |
| Y | 99 | 8 | 8 | 82 | 16 | 19 | 86 | 9 | 11 |
| Zr | 34 | 2 | 5 | 44 | 11 | 25 | 39 | 4 | 11 |
| Nb | 33 | 2 | 5 | 27 | 1 | 5 | 28 | 3 | 10 |
| Cs | < 0.01 | – | – | 0.15 | 0.42 | 277 | 0.04 | 0.03 | 92 |
| Ba | 11.4 | 3.4 | 30 | 57.8 | 38.8 | 67 | 35.9 | 15.5 | 43 |
| La | 50 | 2 | 3 | 45 | 2 | 5 | 51 | 6 | 13 |
| Ce | 163 | 4 | 3 | 131 | 7 | 5 | 146 | 7 | 5 |
| Nd | 100 | 4 | 4 | 94 | 22 | 23 | 97 | 12 | 12 |
| Sm | 19.5 | 1.8 | 9 | 21 | 6.5 | 31 | 21.5 | 4.8 | 22 |
| Eu | 2.4 | 0.3 | 11 | 3.7 | 1.0 | 26 | 3.7 | 0.7 | 18 |
| Gd | 15.5 | 1.2 | 8 | 17.2 | 5.1 | 30 | 18.1 | 4.1 | 23 |
| Dy | 15.5 | 1.6 | 10 | 15.7 | 4.2 | 27 | 15.8 | 3.2 | 20 |
| Er | 10 | 0.7 | 7 | 8.2 | 1.5 | 18 | 8.7 | 1.3 | 15 |
| Yb | 12.2 | 1.1 | 9 | 8.6 | 1.1 | 13 | 9.1 | 0.03 | 0.30 |
| Hf | 2.4 | 0.3 | 11 | 2.7 | 0.5 | 19 | 2.4 | 0.2 | 9 |
| Ta | 0.61 | 0.04 | 6 | 0.58 | 0.11 | 19 | 0.53 | 0.2 | 40 |
| Pb | 1.11 | 0.21 | 19 | 1.35 | 0.32 | 23 | 1.25 | 0.14 | 11 |
| Th | 0.15 | 0.06 | 40 | 0.23 | 0.06 | 27 | 0.42 | 0.1 | 23 |
| U | 0.05 | 0.03 | 69 | 0.09 | 0.08 | 96 | 0.12 | 0.04 | 31 |

**Table 5** Trace element concentrations (ppm) in biotites from the Fish Canyon magmatic system

| | BFC 83 (PPD) | | | Bfc 113 (FCT-O) | | | Bfc 191 (FCT-I) | | |
|---|---|---|---|---|---|---|---|---|---|
| | Average, $N=5$ | SD | Rel. SD (%) | Average, $N=6$ | SD | Rel. SD (%) | Average, $N=3$ | SD | Rel. SD (%) |
| Li | 37 | 4 | 11 | 75 | 13 | 18 | 14 | 1 | 5 |
| P | 23 | 21 | 89 | 20 | 22 | 113 | 6 | 6 | 100 |
| S | 14 | 3 | 19 | 21 | 4 | 19 | n.m. | n.m. | n.m. |
| Sc | 9.0 | 0.6 | 6 | 9.9 | 0.7 | 7 | 11.1 | 1.0 | 9 |
| Cr | 7 | 1 | 16 | 8 | 3 | 34 | 40 | 28 | 71 |
| Ni | 22 | 2 | 9 | 31 | 1 | 5 | 24 | 1 | 5 |
| Rb | 343 | 21 | 6 | 469 | 13 | 3 | 363 | 9 | 3 |
| Sr | 9.0 | 2.1 | 24 | 8.7 | 1.2 | 14 | 10.5 | 1.3 | 12 |
| Y | 0.16 | 0.12 | 75 | 0.08 | 0.04 | 46 | 0.15 | 0.04 | 25 |
| Zr | 3.6 | 1.3 | 35 | 3.4 | 0.4 | 11 | 4.1 | 0.2 | 6 |
| Nb | 36.7 | 1.7 | 5 | 46.7 | 0.5 | 1 | 47 | 2.6 | 5 |
| Cs | 2.7 | 0.3 | 12 | 3.1 | 0.3 | 8 | 2.5 | 1.3 | 50 |
| Ba | 1,554 | 257 | 17 | 1,613 | 291 | 18 | 2,767 | 839 | 30 |
| La | 0.35 | 0.68 | 193 | 0.02 | 0.02 | 114 | 0.06 | 0.06 | 105 |
| Ce | 0.72 | 1.06 | 147 | 0.13 | 0.19 | 141 | 0.13 | 0.15 | 114 |
| Nd | 0.19 | 0.28 | 149 | $<0.01$ | – | – | 0.05 | 0.03 | 59 |
| Sm | $<0.01$ | – | – | $<0.01$ | – | – | $<0.01$ | – | – |
| Eu | 0.06 | 0.02 | 39 | 0.1 | 0.02 | 23 | 0.1 | 0.02 | 15 |
| Gd | 0.07 | 0.04 | 50 | 0.05 | 0.07 | 136 | 0.45 | 0.17 | 39 |
| Dy | $<0.02$ | – | – | 0.03 | 0.03 | 100 | $<0.01$ | – | – |
| Er | $<0.01$ | – | – | $<0.01$ | – | – | $<0.01$ | – | – |
| Yb | 0.05 | 0.02 | 37 | 0.02 | 0.03 | 221 | 0.03 | 0.01 | 30 |
| Hf | 0.28 | 0.06 | 20 | 0.42 | 0.13 | 32 | 0.37 | 0.07 | 20 |
| Ta | 0.9 | 0.1 | 12 | 1.17 | 0.06 | 5 | 1.17 | 0.06 | 5 |
| Pb | 2.02 | 0.37 | 18 | 1.87 | 0.19 | 10 | 1.67 | 0.07 | 4 |
| Th | 0.17 | 0.31 | 183 | 0.02 | 0.03 | 138 | $<0.01$ | – | – |
| U | 0.1 | 0.13 | 140 | 0.11 | 0.09 | 79 | 0.03 | 0.02 | 66 |

**Table 6** Trace element concentrations (ppm) in titanites from the Fish Canyon magmatic system

| | Bfc 15 (PPD) | | | GrdX2 (Grd. xenolith) | | |
|---|---|---|---|---|---|---|
| | Average, $N=9$ | SD | Rel. SD (%) | Average, $N=17$ | SD | Rel. SD (%) |
| Li | 1.3 | 1.1 | 83 | 1.8 | 1.9 | 103 |
| P | 301 | 37 | 12 | 262 | 56 | 22 |
| S | 14.8 | 11.9 | 80 | $<0.01$ | – | – |
| Sc | 17.6 | 2.9 | 17 | 21.8 | 8.2 | 38 |
| Cr | 3.2 | 8.2 | 255 | 22.4 | 12.7 | 57 |
| Fe | 13,740 | 1,327 | 10 | 15,600 | 1,956 | 13 |
| Ni | 0.07 | 1.1 | 1,544 | 0.48 | 0.83 | 171 |
| Rb | 0.31 | 0.16 | 50 | 8.64 | 4.23 | 49 |
| Sr | 35 | 1.5 | 4 | 31.6 | 7.7 | 24 |
| Y | 4,166 | 690 | 17 | 5,022 | 885 | 18 |
| Zr | 767 | 118 | 15 | 864 | 28 | 3 |
| Nb | 1,916 | 37 | 2 | 2,271 | 260 | 11 |
| Cs | 0.01 | 0.03 | 429 | 5.81 | 2.88 | 50 |
| Ba | 0.1 | 0.26 | 260 | 2.71 | 1.5 | 55 |
| La | 3,877 | 243 | 6 | 4,199 | 379 | 9 |
| Ce | 10,330 | 834 | 8 | 11,152 | 1,372 | 12 |
| Nd | 6,392 | 474 | 7 | 7,074 | 927 | 13 |
| Sm | 1,241 | 126 | 10 | 1,334 | 139 | 10 |
| Eu | 201 | 10 | 5 | 182 | 20 | 11 |
| Gd | 968 | 132 | 14 | 1,053 | 92 | 9 |
| Dy | 834 | 119 | 14 | 928 | 114 | 12 |
| Er | 433 | 64 | 15 | 513 | 88 | 17 |
| Yb | 407 | 50 | 12 | 499 | 99 | 20 |
| Hf | 52 | 9 | 18 | 62 | 6 | 10 |
| Ta | 164 | 17 | 10 | 214 | 30 | 14 |
| Pb | 2.12 | 0.23 | 11 | 27.1 | 12.4 | 46 |
| Th | 400 | 46 | 12 | 451 | 54 | 12 |
| U | 59.4 | 5.7 | 10 | 72.4 | 9.9 | 14 |

Grd xenolith = co-magmatic granodioritic xenolith.

**Table 7** Trace element concentrations (ppm) in zircons from the Fish Canyon magmatic system

| | Bfc 15 (PPD) | | | GrnX (Grn. xenolith) | | |
|---|---|---|---|---|---|---|
| | Average, $N=6$ | SD | Rel. SD (%) | Average, $N=7$ | SD | Rel. SD (%) |
| Sc | 478 | 19 | 4 | 415 | 48 | 12 |
| Cr | 1.79 | 1.08 | 60 | 2.28 | 1.32 | 58 |
| Sr | 1.31 | 0.43 | 33 | 1.88 | 1.58 | 84 |
| Y | 1,193 | 425 | 36 | 976 | 424 | 43 |
| Sn | 0.66 | 0.19 | 28 | 0.40 | 0.11 | 43 |
| Zr | 82,979 | 3,898 | 5 | 69,540 | 6,684 | 10 |
| Nb | 30.9 | 1.4 | 4 | 27.2 | 2.8 | 10 |
| Ba | 1.8 | 1.4 | 77 | 2.2 | 2.3 | 106 |
| La | 2.79 | 2.54 | 91 | 7.87 | 10.00 | 127 |
| Ce | 51.2 | 9.9 | 19 | 55.3 | 20.5 | 37 |
| Nd | 4.1 | 1.7 | 42 | 10.1 | 12.0 | 119 |
| Sm | 4.4 | 2.4 | 55 | 5.5 | 4.0 | 72 |
| Eu | 1.32 | 0.77 | 59 | 1.55 | 1.23 | 80 |
| Gd | 22.4 | 12.9 | 58 | 21.3 | 14.8 | 70 |
| Dy | 94.3 | 46.1 | 49 | 83.0 | 49.4 | 60 |
| Er | 186 | 69 | 37 | 148 | 66 | 44 |
| Yb | 481 | 114 | 24 | 372 | 102 | 27 |
| Hf | 9,967 | 1,425 | 14 | 7,669 | 1,348 | 18 |
| Ta | 1.38 | 0.19 | 14 | 1.04 | 0.40 | 38 |
| Pb | 1.18 | 0.56 | 47 | 1.01 | 0.87 | 87 |
| Th | 226 | 48 | 21 | 140 | 52 | 37 |
| U | 413 | 97 | 24 | 274 | 146 | 54 |

Grn. xenolith = co-magmatic granitic xenolith

**Table 8** Trace element concentrations (ppm) in magnetites from the Fish Canyon magmatic system

| | Bfc113 (FCT-O) | | |
|---|---|---|---|
| | Average, $N=2$ | SD | Rel. SD (%) |
| Sc | 6.16 | 0.64 | 10 |
| Cr | 237 | 179 | 75 |
| Co | 97.0 | 2.4 | 2 |
| Ni | 24.0 | 0.3 | 1 |
| Y | 0.20 | 0.05 | 24 |
| Zr | 4.27 | 0.24 | 6 |
| Nb | 5.44 | 0.21 | 4 |
| La | 0.50 | 0.21 | 43 |
| Ce | 0.70 | 0.23 | 34 |
| Pr | 0.08 | 0.02 | 22 |
| Nd | 0.45 | 0.04 | 9 |
| Sm | 0.14 | 0.19 | 141 |
| Gd | 0.09 | 0.12 | 141 |
| Dy | $<0.01$ | – | – |
| Yb | $<0.01$ | – | – |
| Pb | 3.29 | 1.56 | 47 |

$TiO_2$ was 5.1 wt%. Most analyses had much higher concentrations of REE (up to 250 ppm Ce and 100 ppm Nd). We interpret these high values as manifestations of titanite, zircon and/or apatite inclusions.

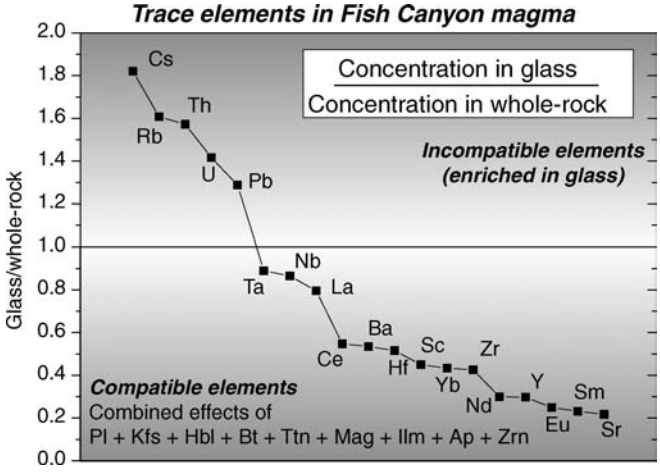


**Fig. 1** Ratios of average trace element concentration in glass vs. concentration in the whole rock (Pagosa Peak Dacite pumice; Bfc 83; Bachmann et al. 2002) for multiple elements in the Fish Canyon magmatic system, showing the elements enriched in the glass compared to the whole rock (incompatible elements with the assemblage Pl + Kfs + Hbl + Bt + Ttn + Mag + Ilm + Ap + Zrn), and those which are depleted (compatible elements). Note that Y and HREE are almost as compatible as Sr, and more compatible than Ba

coefficients for the relevant phases (see, for example, the compilation by Rollinson 1993). Particularly striking are the values for REE and Y in titanite, which are 10–50 times higher than recently published partition coefficients for a lamproitic magma (Tiepolo et al. 2002; Fig. 2a). $\check{C}_{HREE}/\check{C}_{LREE}$ in Fish Canyon titanite are also much higher than $D_{HREE}/D_{LREE}$ in titanite of the lamproitic magma. The values of $\check{C}_{REE\text{-titanite}}$ are probably not overestimated, as similarly REE-enriched titanites can be found in other silicic magmatic rocks (Paterson et al. 1989; Nakada 1991; Della Ventura et al. 1999). $\check{C}_{REE}$ for hornblende are also higher than most literature values (Fig. 2b; Rollinson 1993; Sisson 1994). In comparison to the data of Mahood and Hildreth (1983), $\check{C}_{REE}$ for Fish Canyon biotite are much lower than in the Bishop Tuff, perhaps reflecting the competition of hornblende and titanite for these elements in the Fish Canyon magma (Fig. 3, see Ren et al. 2003 for a similar

**Table 9** $\check{C}_{i\text{-min}}/\check{C}_{i\text{-melt}}$ for the Fish Canyon magmatic system

| | Plagioclase | Sanidine | Biotite | Hornblende | Titanite | Zircon | Magnetite |
|---|---|---|---|---|---|---|---|
| Li | 0.2 | 0.01 | 1.2 | 0.3 | 0.04 | n.c. | n.c. |
| S | 0.9 | 0.3 | 1.6 | 1.1 | 1.34 | n.c. | n.c. |
| Sc | 0.5 | 0.5 | 3.4 | 45 | 5.9 | 161 | 2.1 |
| Cr | 5.4 | < 0.01 | 99.3 | 20.6 | 17.6 | 9.73 | 1,290 |
| Fe | 0.5 | 0.2 | 25 | 22 | 2.95 | n.c. | n.c. |
| Ni | 2.8 | 0.3 | 92 | 45 | 0.26 | n.c. | 86 |
| Rb | < 0.01 | 0.7 | 2.0 | 0.0 | < 0.01 | n.c. | n.c. |
| Sr | 12.5 | 7.4 | 0.1 | 0.4 | 0.37 | 0.01 | n.c. |
| Y | 0.02 | 0.1 | 0.02 | 13.5 | 633 | 181 | 0.03 |
| Zr | < 0.01 | < 0.01 | 0.05 | 0.5 | 9.64 | 1,043 | 0.05 |
| Nb | < 0.01 | < 0.01 | 2.9 | 2.0 | 129 | 2.09 | 0.37 |
| Cs | < 0.01 | 0.02 | 0.5 | 0.01 | < 0.01 | n.c. | n.c. |
| Ba | 0.61 | 17.1 | 4.4 | 0.08 | < 0.01 | < 0.01 | n.c. |
| La | 0.4 | 0.06 | < 0.01 | 1.4 | 113 | 0.1 | 0.01 |
| Ce | 0.3 | 0.02 | 0.01 | 3.2 | 223 | 1.10 | 0.01 |
| Nd | 0.2 | < 0.01 | 0.01 | 9.7 | 639 | 0.41 | 0.04 |
| Sm | 0.1 | < 0.01 | < 0.01 | 15.5 | 930 | 3.28 | 0.10 |
| Eu | 3.1 | 2.9 | 0.3 | 10.8 | 661 | 4.35 | n.c. |
| Gd | 0.08 | 0.1 | 0.2 | 14.9 | 855 | 19.8 | 0.08 |
| Dy | 0.02 | < 0.01 | 0.01 | 17.6 | 935 | 106 | n.c. |
| Er | < 0.01 | 0.01 | 0.02 | 13.2 | 636 | 274 | n.c. |
| Yb | 0.01 | 0.03 | 0.03 | 9.6 | 393 | 465 | n.c. |
| Hf | < 0.01 | 0.1 | 0.1 | 0.9 | 18.7 | 3,580 | n.c. |
| Ta | < 0.01 | 0.3 | 1.0 | 0.5 | 153 | 1.29 | n.c. |
| Pb | 0.5 | 1.1 | 0.1 | 0.1 | 0.10 | 0.05 | 0.15 |
| Th | < 0.01 | < 0.01 | < 0.01 | 0.01 | 18.7 | 10.6 | n.c. |
| U | 0.019 | < 0.01 | < 0.01 | 0.01 | 7.0 | 48.6 | n.c. |

Data were calculated using an average of three samples for plagioclase, sanidine, biotite, and hornblende, of two samples for titanite and zircon, and of one sample for magnetite. *n.c.* not calculated. Co and Pr were both measured in magnetite but not in the glass and are, therefore, not reported

**Table 10** Comparison of petrographic modes (determined by point counting; Bachmann et al. 2002) with calculated modes (see footnotes and text for details)

| | Pl | Kfs | Bt | Hbl | Ttn | Glass |
|---|---|---|---|---|---|---|
| Petrographic mode | 26 | 6 | 3.5 | 4 | 0.7 | 56 |
| Calculated average mode | 26 | 4 | 2.9 | 2.5 | 0.6 | 59 |
| Ba (ppm) | 311 | 5,636 | 1,584 | 35 | 1 | 447 |
| Mode (calc.) | 26% | 3% | 3.2% | 3.5% | 1% | 59% |
| Sr (ppm) | 1,189 | 519 | 9 | 40 | 33 | 95 |
| Mode (calc.) | 30% | 5.8% | 3.5% | 3.6% | 1.1% | 60% |
| Rb (ppm) | 2 | 97 | 406 | 3 | 4 | 193 |
| Mode (calc.) | 26% | 2.8% | 0.9% | 0.5% | 0.9% | 57% |
| Pb (ppm) | 11 | 17 | 2 | 1 | 15 | 22 |
| Mode (calc.) | 26% | 3.8% | 3.5% | 3.5% | 0.1% | 60% |
| Y (ppm) | 0.1 | 0.4 | 0.1 | 89 | 4,165 | 6.6 |
| Mode (calc.) | 26% | 4.1% | 3.5% | 3.5% | 0.4% | 59% |
| Ce (ppm) | 12.4 | 1 | 0.4 | 146 | 10,330 | 46.4 |
| Mode (calc.) | 26% | 4.2% | 3.5% | 3.5% | 0.5% | 59% |

For each of the elements listed above, calculated modes were determined by least-squares fitting (using the MS Excel solver) the proportions of the different minerals and melt, when multiplied by their average trace element contents and summed to the whole-rock concentration (i.e., for Ba: $X_{Pl}{}^{*}\check{C}_{Ba-Pl} + X_{Kfs}{}^{*}\check{C}_{Ba\text{-}Kfs} + X_{Bt}{}^{*}\check{C}_{Ba\text{-}Bt} + X_{Hbl}{}^{*}\check{C}_{Ba\text{-}Hbl} + X_{Ttn}{}^{*}\check{C}_{Ba\text{-}Ttn} + X_{Glass}{}^{*}\check{C}_{Ba\text{-}Glass}$ = whole-rock concentration)

hypothesis for Ba and Sr partitioning in magmas containing both plagioclase and sanidine). Alternatively, the lower partitioning ratios in the biotites of the Fish Canyon magma compared to those of the Bishop Tuff could be due to different major element compositions (of both the biotites and the melt).

## Trace-element zoning in hornblende

As mentioned in the previous section, trace element zoning is generally difficult to resolve by laser-ablation techniques due to the large spot size of the laser with respect to the size of crystals and the dimensions of individual zones. However, one large hornblende (~2 mm diameter), for which major element zoning has been reported in Bachmann and Dungan (2002; Hornblende Fig. 2b), was sufficiently large for a six-point core-to-rim traverse (Fig. 4). This traverse records rimward *increases* (by factors of 4–6) for the feldspar-compatible elements Sr and Ba and significant rimward *decreases* in the hornblende- and titanite-compatible elements Sc and Ce. Other elements, such as Nd, Y, and La, which are compatible with hornblende and titanite,

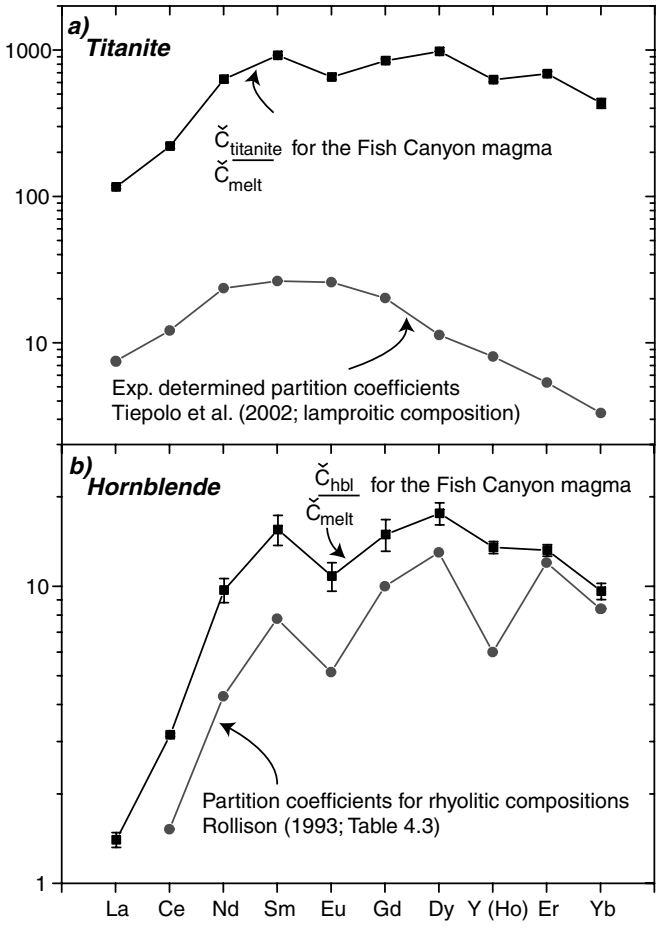


**Fig. 2** Index of partitioning behavior ($\check{C}_{i\text{-}min.}/\check{C}_{i\ melt}$) for the Fish Canyon titanite **a** and hornblende **b** compared to published equilibrium partition coefficients (*D*)

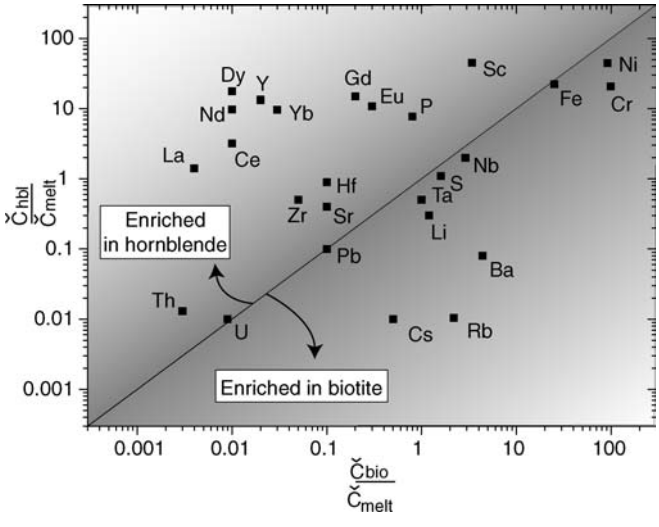


**Fig. 3** Partitioning behavior of selected trace elements for the Fish Canyon biotite plotted against that for hornblende, illustrating the trace element "preference" of each phase

also decrease by 10–20% toward the rim (Fig. 4). Europium shows a nominal two-fold enrichment toward the rim (from 2 to 4 ppm), but in light of its low concentration, our data have large analytical uncertainties.

## Discussion

### HREE and Y depletions in the melt: a "garnet-like" signature forged in a shallow magmatic hearth

Depletions of HREE and Y in magmas are commonly interpreted in terms of magma generation (by partial melting) or differentiation (by crystal fractionation) in the garnet stability field. For example, Hildreth and Moorbath (1988) inferred that high La/Yb, Ce/Yb, and La/Y in Quaternary Andean arc magmas are the signature of evolution near the base of a thick crust where garnet was stable. LREE/HREE in the Fish Canyon glass are close to the values in these Andean magmas and are elevated compared to the whole-rock composition (Table 11). In the case of the Fish Canyon magma, the differentiation of the interstitial liquid occurred at shallow depth (~2.5 kb, Johnson and Rutherford 1989; Bachmann and Dungan 2002), precluding garnet crystallization in the Fish Canyon magma chamber.

As previously suggested by Frey et al. (1978), mineral phases other than garnet can lead to depletions in Y and HREE in upper crustal granitoid batholiths. We favor such an alternative hypothesis wherein the depletions of Y and HREE in Fish Canyon glass are the consequence of modally abundant hornblende and titanite (+ much less abundant zircon) that preferentially incorporate these elements. In addition, the high degree of polymerization (i.e., high mole fraction of network-forming components) and low temperature of the high-$SiO_2$ rhyolite melt almost certainly contributed to increased trace element compatibility in such crystalline phases (see Mahood and Hildreth 1983; Nash and Crecraft 1985). Although hornblende and titanite together comprise about 10% of the phenocryst assemblage (Table 10), these modal abundances and the high compatibilities of Y and HREE (Table 9) are sufficient to deplete these elements in residual melt.

A trace element ratio that is widely used to estimate depth of differentiation is Sr/Y, as it provides a proxy for the plagioclase/garnet ratio in the crystalline residue (e.g., Defant and Drummond 1990; Drummond and Defant 1990; Garrison and Davidson 2003; Tulloch and Kimbrough 2003). Fish Canyon glasses have Sr/Y of 13–18, which is lower than the value for the Fish Canyon magma (whole-rock Sr/Y ~17–24), and lower than the value of 40 that is usually accepted as the minimum for high Sr/Y ("adakitic") magmas (e.g., Tulloch and Kimbrough 2003). Therefore, the typical upper crustal mineral assemblage in silicic magmas is apparently not capable of significantly increasing Sr over Y, even where feldspars have been resorbed, and high Sr/Y ratios (> 40) remain a valuable indication of

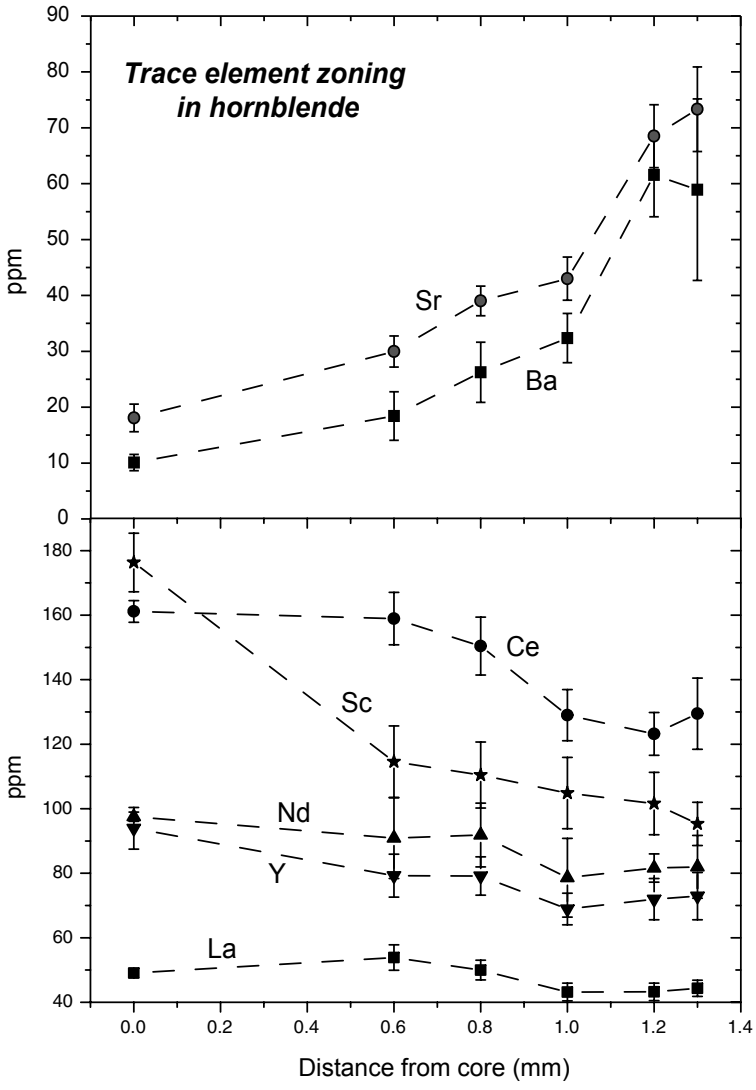


**Fig. 4** Core-to-rim traverse in a 2-mm-long hornblende (Hornblende b, in Fig. 2 of Bachmann and Dungan 2002), documenting significant trace element zoning. Errors are 1 $\sigma$. Relative standard deviations (in %) of analyses of the USGS basalt glass standard BCR2g, used as a monitor during analytical sessions, are $\pm$1.5% for Sr, 1.6% for Ba, 4.0% for Sc, 1.7% for Ce, 2.6% for Nd, 4.7% for Y, and 2.0% for La

**Table 11** Comparison of trace element ratios between the Fish Canyon magma (glass and whole rock) and other silicic units thought to have evolved in the garnet stability field

| | FC magma | FC Glass | HISY | SVZ |
|---|---|---|---|---|
| La/Y | ~2 | ~5 | 0.4–7 | – |
| La/Yb | 18–21 | 32–35 | Up to 40 | – |
| Ce/Yb | 33–39 | 42–49 | – | 30–40 |
| Ba/La | 17–22 | 10–15 | – | 35–50 |
| Sr/Y | 17–24 | 13–18 | 45–260 | – |

HISY = High Sr/Y magmas of Tulloch and Kimbrough (2003). SVZ = Southern Volcanic Zone of the Andes (Hildreth and Moorbath 1988)

the influence of garnet during magma generation and/or differentiation.

## Evolution of the melt composition

In accord with several lines of evidence enumerated by Bachmann et al. (2002) and Bachmann and Dungan (2002), we interpret the observed Sr and Ba zoning profiles in Fish Canyon hornblende (Fig. 4) as the consequence of increases in these elements in the melt during hornblende crystallization due to dissolution of feldspars. We have considered the possibility that partition coefficients for these elements changed during the crystallization of hornblende due to crystal-chemical and thermal effects as Fish Canyon hornblendes record significant major element zoning (in particular, a typical 30% rimward increase in $^{iv}$Al indicative of reheating from ~715 to 760°C during crystallization). If the interpretation that the rims crystallized at higher temperature than the cores is correct, partition coefficients would have been lower at the rim (Blundy and Wood 2003), leading to decreasing Sr and Ba toward the rim. The effect of major element variations on the trace element partitioning in complex minerals such as hornblende is less well constrained. It is, however, possible to draw analogies with calcic pyroxenes, in which partition coefficients are thought to respond to major element variations in a similar manner to hornblende (Klein

et al. 1997; Bottazi et al. 1999). Hill et al. (2000) showed that partition coefficients for alkaline earths (such as Sr and Ba) in clinopyroxenes do not vary significantly with increasing $^{iv}$Al. Moreover, one would expect that major element variations in the M4 site, the most likely host of Sr (and, to a lesser extent, Ba) in hornblende, should be most critical in generating crystal-chemical effects on $D_{Sr}$ and $D_{Ba}$. In Fish Canyon hornblendes, Ca fills more than 90% of the M4 site, and it is the only major element that remains nearly constant from cores to rims (Bachmann and Dungan 2002). Consequently, there is no evidence that the combined thermal and crystal-chemical effects could lead to such large and systematic rimward enrichments in these elements over a distance greater than 1 mm, nor do we conclude that kinetic factors related to boundary layer diffusion around growing hornblendes in this "plutonic" environment could be important. In agreement with the hypothesis of evolving melt composition, rimward depletions in REE, Y and Sc reflect the compatible behavior of these elements in the Fish Canyon crystalline assemblage.

## Conclusions

The interstitial glass present in multiple units of the Fish Canyon magmatic system is characterized by marked depletions of HREE and Y with respect to whole-rock compositions, in combination with relatively high concentrations of Ba and Sr when compared to other high-$SiO_2$ rhyolites such as the Bishop Tuff-Glass Mountain system (Metz and Mahood 1991), Bearhead Rhyolite (Justet and Spell 2001), Bandelier Tuff (Wolff et al. 1999), Yellowstone (Table 4 of Hildreth et al. 1991), Toconao ignimbrite (Table 7 of Lindsay et al. 2001), and Taylor Creek Rhyolite (Knesel et al. 1999). An assessment of the trace element budget in this magmatic system indicates that this signature is a consequence of: (1) the low temperature (700–760°C) and the highly polymerized nature of the Fish Canyon interstitial melt, leading to elevated partition coefficients, and (2) the high modal abundance of hornblende + titanite, which strongly partitioned HREE and Y into the crystalline portion of the system. This assemblage, rare in crystal-poor volcanic rocks (Nakada 1991; Deer et al. 1992) but common in monotonous intermediate ignimbrites (Lindsay et al. 2001; Bachmann et al. 2002; Maughan et al. 2002) and in granodiorite batholiths (e.g., Bateman and Chappell 1979), controls the budget of certain trace elements (see Frey et al. 1978; Watson and Harrison 1984; Bea 1996 for similar conclusions) and may produce a "garnet-like" signature, with high LREE/HREE and LREE/Y in the late-stage melt (e.g., Ce/Yb > 40 and La/Y > 5).

Trace element zoning in a hornblende phenocryst supports the conclusion that the Fish Canyon magma was thermally rejuvenated prior to eruption by the dissolution of feldspars and quartz, which was accompanied by the growth of hornblende, titanite and biotite. This inference, first made on the basis of textural and geochemical arguments (Bachmann and Dungan 2002; Bachmann et al. 2002), is consistent with the four- to six-fold rimward increases in Sr and Ba in hornblende by addition of these elements to the melt during feldspar resorption. Variations in partition coefficients for these elements due to major element zoning in hornblende may have played some role in producing these trace element zonations, but are unlikely to be the major factor. Despite the addition of Sr to the interstitial melt during magma rejuvenation, the ratio of feldspar dissolution over crystallization of amphibole + titanite (±zircon) was not sufficient to increase the Sr/Y ratio to the "adakitic" level (Sr/Y > 40). Therefore, Sr/Y remains a valuable criterion for determining the depth of magma generation and/or differentiation in an arc setting.

**Acknowledgments** As for all our papers on the Fish Canyon magmatic system, we are deeply indebted to Peter Lipman for his long-term support and collaboration. This project was supported by the Swiss NSF grant# 20–49730.96 to M.A. Dungan. We thank Mark Schmitz and an anonymous reviewer for constructive reviews of an earlier version of this manuscript and Tim Grove for efficient editorial handling.

## References

Bachmann O, Bergantz GW (2003) Rejuvenation of the Fish Canyon magma body: a window into the evolution of large-volume silicic magma systems. Geology 31(9):789–792

Bachmann O, Dungan MA (2002) Temperature-induced Al-zoning in hornblendes of the Fish Canyon magma, Colorado. Am Mineral 87:1062–1076

Bachmann O, Dungan MA, Lipman PW (2000) Voluminous lava-like precursor to a major ash-flow tuff: low-column pyroclastic eruption of the Pagosa Peak Dacite, San Juan Volcanic field, Colorado. J Volcanol Geotherm Res 98:153–171

Bachmann O, Dungan MA, Lipman PW (2002) The Fish Canyon magma body, San Juan volcanic field, Colorado: rejuvenation and eruption of an upper crustal batholith. J Petrol 43(8):1469–1503

Bachmann O, Oberli F, Dungan MA, Meier M, Fischer H (submitted to Chemical Geology) $^{40}$ Ar/$^{39}$ Ar and U-Pb dating of the Fish Canyon magmatic system, San Juan Volcanic field, Colorado: evidence for an extended crystallization history

Bateman PC, Chappell BW (1979) Crystallization, fractionation, and solidification of the Tuolumne Intrusive Series, Yosemite National Park, California. Geol Soc Am Bull 90:465–482

Bea F (1996) Residence of REE, Y, Th, and U in granites and crustal protoliths; implications for the chemistry of crustal melts. J Petrol 37:521–552

Blundy J, Wood B (2003) Partitioning of trace elements between crystals and melts. Earth Planet Sci Lett 210(3–4):383–397

Bottazi P, Tiepolo M, Vannucci R, Zanetti A, Brumm R, Foley SF, Oberti R (1999) Distinct site preferences for heavy and light REE in amphibole and the prediction of $^{Amph/L}$ $D_{REE}$. Contrib Mineral Petrol 137:36–45

Deer WA, Howie RA, Zussman J (1992) An introduction to the rock-forming minerals, 2nd edn. Longman Group Ltd, New York, p 698

Defant MJ, Drummond MS (1990) Derivation of some modern arc magmas by melting of young subducted lithosphere. Nature 347:662–665

Della Ventura G, Bellatrecia F, Williams CT (1999) Zr- and LREE-rich titanite from Tre Croci, Vico Volcanic complex, (Latium, Italy). Mineral Mag 63:123–136

Devine JD, Rutherford MJ, Norton GE, Young SR (2003) Magma storage region processes inferred from geochemistry of Fe–Ti oxides in andesitic magma, Soufrière Hills volcano, Montserrat, WI. J Petrol 44(8):1375–1400

Drummond MS, Defant MJ (1990) A model for trondhjemite–tonalite–dacite genesis and crustal growth via slab melting: Archean to Modern comparison. J Geophys Res 95:21503–21521

Frey FA, Chappell BW, Stephen DR (1978) Fractionation of rare-earth elements in the Tuolumne Intrusive Series. Geology 6:239–242

Garrison JM, Davidson JP (2003) Dubious case for slab melting in the Northern volcanic zone of the Andes. Geology 31:565–568

Hildreth W (1981) Gradients in silicic magma chambers: implications for lithospheric magmatism. J Geophys Res 86(B11):10153–10192

Hildreth W, Halliday AN, Christiansen RL (1991) Isotopic and chemical evidence concerning the genesis and contamination of basaltic and rhyolitic magma beneath the Yellowstone Plateau volcanic field. J Petrol 32(1):63–137

Hildreth WS, Moorbath S (1988) Crustal contributions to arc magmatism in the Andes of Central Chile. Contrib Mineral Petrol 98:455–499

Hill E, Wood BJ, Blundy JD (2000) The effect of Ca-Tschermaks component on trace element partitioning between clinopyroxene and silicate melt. Lithos 53(3–4):203–215

Irving AJ, Frey FA (1978) Distribution of trace elements between garnet megacrysts and host volcanic liquids of kimberlitic to rhyolitic composition. Geochim Cosmochim Acta 42:771–788

Irving AJ, Frey FA (1984) Trace element abundances in megacrysts and their host basalts: constraints in partition coefficients and megacryst genesis. Geochim Cosmochim Acta 48:1201–1221

Johnson M, Rutherford M (1989) Experimentally determined conditions in the Fish Canyon Tuff, Colorado, magma chamber. J Petrol 30:711–737

Justet L, Spell TL (2001) Effusive eruptions from a large silicic magma chamber: the Bearhead Rhyolite, Jemez volcanic field, NM. J Volcanol Geotherm Res 107:241–264

Klein M, Stosch H-G, Seck HA (1997) Partitioning of high field-strength and rare-earth elements between amphibole and quartz-dioritic to tonalitic melts: an experimental study. Chem Geol 138(3–4):257–271

Knesel KM, Davidson JP, Duffield WA (1999) Evolution of silicic magma through assimilation and subsequent recharge: evidence from Sr isotopes in sanidine phenocrysts, Taylor Creek Rhyolite, NM. J Petrol 40(5):773–786

Lindsay JM, Schmitt AK, Trumbull RB, De Silva SL, Siebel W, Emmermann R (2001) Magmatic evolution of the La Pacana caldera system, Central Andes, Chile: Compositional variation of two cogenetic, large-volume felsic ignimbrites. J Petrol 42(3):459–486

Lipman PW (2000) The central San Juan caldera cluster: Regional volcanic framework. In: Bethke PM, Hay RL (eds) Ancient Lake Creede: its volcano-tectonic setting, history of sedimentation, and relation of mineralization in the Creede mining district: Geol Soc Am Spec Pap 346:9–69

Lipman PW, Dungan MA, Bachmann O (1997) Comagmatic granophyric granite in the Fish Canyon Tuff, Colorado: Implications for magma-chamber processes during a large ash-flow eruption. Geology 25(10):915–918

Mahood G, Hildreth W (1983) Large partition coefficients for trace elements in high-silica rhyolites. Geochim Cosmochim Acta 47:11–30

Maughan LL, Christiansen EH, Best MG, Gromme CS, Deino AL, Tingey DG (2002) The Oligocene Lund Tuff, Great Basin, USA: a very large volume monotonous intermediate. J Volcanol Geotherm Res 113:129–157

Metz JM, Mahood GA (1991) Development of the Long Valley, California, magma chamber recorded in precaldera rhyolite lavas of Glass Mountain. Contrib Mineral Petrol 106:379–397

Murphy MD, Sparks RSJ, Barclay J, Carroll MR, Brewer TS (2000) Remobilization of andesitic magma by intrusion of mafic magma at the Soufrière Hills Volcano, Montserrat, West Indies. J Petrol 41(1):21–42

Nakada S (1991) Magmatic processes in titanite-bearing dacites, central Andes of Chile and Bolivia. Am Mineral 76:548–560

Nash WP, Crecraft HR (1985) Partition coefficients for trace elements in silicic magmas. Geochim Cosmochim Acta 49:2309–2322

Paterson BA, Stephens WE, Herd DA (1989) Zoning in granitoid accessory minerals as revealed by backscattered electron imagery. Mineral Mag 53:55–61

Ren M, Parker DF, White JC (2003) Partitioning of Sr, Rb, Y, and LREE between plagioclase and peraluminous silicic magma. Am Mineral 88:1091–1103

Rollinson H (1993) Using geochemical data: evaluation, presentation and interpretation. Longman Scientific, Harlow, 352 pp

Rutherford MJ (2002) Nature and timing of magma interaction processes in arc volcanic systems: data from rocks and from phase experiments. EOS Trans Am Geophys Union 82:47

Rutherford MJ, Devine JD (2003) Magmatic conditions and magma ascent as indicated by hornblende phase equilibria and reactions in the 1995–2002 Soufrière Hills magma. J Petrol 44(8):1433–1453

Schmitz MD, Bowring SA (2001) U–Pb zircon and titanite systematics of the Fish Canyon Tuff. An assessment of high-precision U–Pb geochronology and its application to young volcanic rocks. Geochim Cosmochim Acta 65(15):2571–2587

Sisson TW (1994) Hornblende-melt trace element partitioning measured by ion microprobe. Chem Geol 117(1–4):331–344

Tiepolo M, Oberti R, Vannucci R (2002) Trace-element incorporation in titanite: constraints from experimentally determined solid/liquid partition coefficients. Chem Geol 191(1–3):105–119

Tulloch AJ, Kimbrough DL (2003) Paired plutonic belts in convergent margins and the development of high Sr/Y magmatism: the Peninsular Ranges Batholith of California and the Median Batholith of New Zealand. Geol Soc Am Spec Pap 374:275–295

Watson EB, Harrison TM (1984) Accessory minerals and the geochemical evolution of crustal magmatic systems: a summary and prospectus of experimental approaches. Phys Earth Planet Int 35:19–30

Witt-Eickschen G, Seck HA, Mezger K, Eggins SM, Altherr R (2003) Lithospheric mantle evolution beneath the Eifel (Germany): constraints from Sr–Nd–Pb isotopes and trace element abundances in spinel peridotite and pyroxenite xenoliths. J Petrol 44:1077–1095

Wolff JA, Ramos FC, Davidson JP (1999) Sr isotope disequilibrium during differentiation of the Bandelier Tuff: constraints on the crystallization of a large rhyolitic magma chamber. Geology 27(6):495–498